Physics of Plasmas

Structural transition of vortices to nonlinear regimes in a dusty plasma

Cite as: Phys. Plasmas **25**, 103701 (2018); https://doi.org/10.1063/1.5045772
Submitted: 24 June 2018 . Accepted: 18 September 2018 . Published Online: 08 October 2018

Modhuchandra Laishram, and Ping Zhu

View Online Export Citation CrossMark

ARTICLES YOU MAY BE INTERESTED IN

Methods for the characterization of imposed, ordered structures in MDPX
Physics of Plasmas **25**, 103702 (2018); https://doi.org/10.1063/1.5049594

Experimental observation of cnoidal waveform of nonlinear dust acoustic waves
Physics of Plasmas **25**, 113701 (2018); https://doi.org/10.1063/1.5046402

Dust shedding from a dielectric surface in plasma as a result of charge fluctuations
Physics of Plasmas **25**, 103703 (2018); https://doi.org/10.1063/1.5029562

AIP Publishing

© 2018 Author(s).

Structural transition of vortices to nonlinear regimes in a dusty plasma

Modhuchandra Laishram[1] and Ping Zhu[1,2,3]
[1]CAS Key Laboratory of Geospace Environment and Department of Engineering and Applied Physics, University of Science and Technology of China, Hefei 230026, China
[2]KTX Laboratory and Department of Engineering and Applied Physics, University of Science and Technology of China, Hefei 230026, China
[3]Department of Engineering Physics, University of Wisconsin-Madison, Madison, Wisconsin 53706, USA

(Received 24 June 2018; accepted 18 September 2018; published online 8 October 2018)

The structural transition of a steady state dust flow from linear to nonlinear regimes is analyzed using a two-dimensional hydrodynamic model for the dust fluid confined in an axisymmetric toroidal system along with an unbounded streaming plasma. Numerical solutions of the employed hydrodynamical model not only confirms the analytical structure of the driven dust vortex flow in the linear limit as reported in the previous analysis but also shows how the dust vortices are strongly affected by the nonlinear convective transport of the flow at the higher Reynolds number (Re) regime. Effects of various system parameters including external driving field and the Reynolds number are investigated within the linear to nonlinear transition regime $0.001 \leq \mathrm{Re} < 50$. In agreement with relevant experimental observations, the steady flow structure which is symmetric around the center in the linear regime begins to turn asymmetric in the nonlinear regime. The structure of the steady dust flow is found to be influenced mainly by the dissipation scales due to kinematic viscosity, ion drag, and neutral collision in the nonlinear regime, whereas, in the linear regime, it is mainly controlled by the external driving field and the confining boundaries. *Published by AIP Publishing.* https://doi.org/10.1063/1.5045772

I. INTRODUCTION

Vortex or swirling flows about an axis are ubiquitous in most complex fluids involving multiple spatial and temporal scales. The key feature of such complex fluids is the interactions of various constituents that lead to collective behaviors such as self-organization and pattern formation.[1–4] For example, flows in polymer solutions, colloidal suspensions and many biological systems, are complex flows in low Reynolds number regimes that exhibit a vortex or circulating flow pattern.[5–10] On the other hand, similar self-organized vortex flows are also observed in many higher Reynolds number macroscopic flow systems such as White Ovals, Great Red Spot of Jupiter, polar vortex of Earth, and macroscopic circulations including hurricanes and tornadoes in planetary atmospheres.[11–13] The vortex structure in such driven dissipative systems evolves in various dynamical regimes. It has been observed in different sizes, shapes, orientations, aspect ratios, and convection velocities. It has been recognized that the vortex structure plays an important role in fluid mixing and transport process in laminar and turbulent flows.[13,14] Thus, it has been a topic of active research that how the vortical structure evolution in various complex fluid flows depends on system parameters, in particular, the Reynolds number from the viscous dominant linear regime to the inertial dominant nonlinear flow regime. When the flow is viscous dominant which happens mostly at lower flow velocity and smaller length scale ($\mathrm{Re} \leq 1$), the gradients in the hydrostatic pressure are balanced by viscous diffusive producing smooth deformation and laminar flows. However, at higher flow velocity and larger length scale ($\mathrm{Re} \gg 1$), the viscous stress is comparable or less than the inertial convective transport and the pressure gradients act to accelerate the fluid elements and generate nonlinear convective flows.

Interestingly, dust clouds electrostatically suspended in a plasma can be a realizable prototype for experimental or theoretical formulation for various characteristics of driven-dissipative complex fluid flows. Dusty plasma can exist in many states of matter from the collisionless compressible fluid in the weakly coupled regime ($\Gamma \ll 10$) up to the incompressible dust crystalline ($\Gamma \geq \Gamma^* \approx 175$) in the strongly coupled regime.[15] In the strongly coupled regime with the parameter range $10 \leq \Gamma \leq 100$, and for a fixed screening parameter κ, dusty plasma behaves like an incompressible complex fluid which can be modeled using the simplified hydrodynamic Navier-Stokes equations for its flow dynamics. Here, $\Gamma = E_p/E_k$, i.e., the strength of Coulomb potential energy E_p over kinetic energy E_k and the screening parameter $\kappa = d/\lambda_D$, i.e., the ratio of the inter-particle distance over the Debye length due to the background plasma.[15] This flow regime also exhibits many self-organized vortices or circulating flow as collective behaviors due to its long-range Coulomb interactions.[16–18] Recently, the vortex formation and its structural changes with varying the system parameters are observed in some of the dusty plasma experiments which are yet to be fully understood. For example, Mitik *et al.*[19] have observed dust vortex driven by neutral gas convection, and structural variation with a change in pressure and the applied field. In another experiment, Hall *et al.*[20] observed the asymmetric response of dust clouds to a change in the relative strengths of the electrostatic and ion drag forces at varying pressure.

Study of dust vortex structures in such a complex plasma presents an attractive option for analyzing and

interpreting the dynamics of many relevant complex fluids flows in laboratories, industrial applications and many natural processes. In the previous linear (Re $\ll$ 1) analysis,[3,4] the analytic structure of the steady dust flow driven by an unbounded and sheared ion flow is obtained. The scales of the vortex developed in the linear regime mainly depend on those of the ion flow driver, the boundaries, and as various system parameters including the kinematic viscosity. In recent dusty plasma experiments,[21,22] very localized and isolated regions of acceleration and frictional retardation in velocity field, along with a uniform vorticity region surrounded by highly sheared layers of dust vortex motion, are produced. This suggests that the laboratory dusty plasma may have entered the nonlinear regime of the vortex flow and lends itself to the study of macroscopic nonlinear dynamics in such systems of similar Reynolds number.[3] It motivates us to extend the previous linear analysis to the higher Reynolds number flow regime (Re $\gg$ 1), where the nonlinear inertial flow is effective which may explain many new flow characteristics as observed in various dusty plasma experiments.[21]

In the previous work,[23] we developed a 2D numerical model for the dynamics of steady dust fluid flow confined in an axisymmetric toroidal configuration along with an unbounded streaming ions. The previous work focuses on the highly extreme nonlinear regime, in a fixed flow domain of aspect-ratio unity ($L_z/L_r = 1$). Further, the solution of the hydrodynamic model is simply presented without details on the numerical scheme or its validity. In comparison, in the current work we extend the previous work in the following aspects: First, we focus on the linear to nonlinear flow transition regimes. Second, we extend the analysis to a larger domain ($L_z/L_r = 2$) relevant to some of the recent dusty plasma experiments and display the effects of various system parameters in terms of changes in the vortex structure from linear to nonlinear flow regimes. Additionally, we provide and discuss on the numerical procedure for the nonlinear solution of the 2D hydrodynamic model and its validity systematically. This formulation is generic and applicable to the study of many relevant driven-dissipative complex flow systems.

Thus, the manuscript is organized as follows. The 2D hydrodynamic model for the dynamics of driven-dissipative dust fluid recalled from the previous work and the detail procedure for obtaining the numerical solutions are discussed in Sec. II. Then, the dust flow system is characterized in Sec. III, including the benchmark of the numerical solutions in Sec. III A. The structure changes for the steady dust flow from the linear to the nonlinear regime are demonstrated for two cases of an external driving field in Sec. III B. Further, the structure dependence on the system parameters, namely, the kinetic viscosity of the dust fluid μ, the ion dragging co-efficient ξ, and the neutral collision frequency ν are described in Sec. III B. Summary and conclusions are presented in Sec. IV.

II. HYDRODYNAMIC MODEL AND NUMERICAL SOLUTION

We adopt the 2D hydrodynamic model for the dust flow from the previous work.[23] The geometry of confined dust

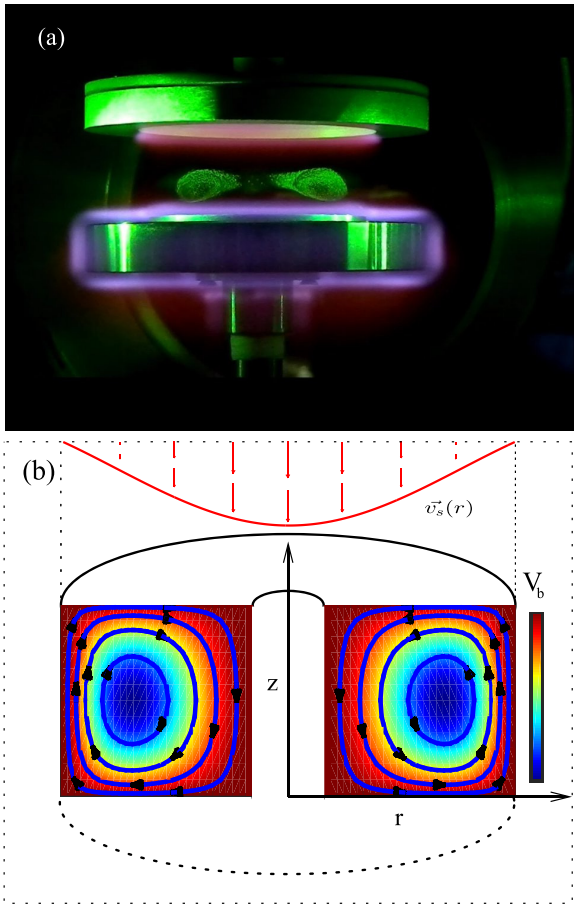

FIG. 1. (a) Toroidal dust clouds with poloidal circulation in the laboratory dusty plasma experimental setup by Kaur *et al.*[21] (b) Schematic representation of dust cloud confined toroidally by the electrostatic potential $V_b(r, z)$ and driven poloidally by the sheared ion flow $v_s(r, z)$ throughout the dust clouds [Reproduced with permission from AIP Conf. Proc. **1925**, 020028 (2018). Copyright 2018 AIP Publishing LLC].

fluid is relevant to the recent laboratory experiment where a toroidal dust cloud flowing in the poloidal direction in a glow discharge plasma, as shown in Fig. 1(a).[21,22] The confinement or the localization of the dust clouds in dynamic equilibrium with the unbounded plasma in most of the laboratory experiments is achieved effectively by a combination of electrostatic and gravitational fields.[24–27] The dust fills volume of a torus which generally acquires a non-regularly shaped cross-section determined by the effective confining potential $\mathbf{F_c} = -\nabla V_b$ in real systems. For analytic or computational simplicity, however, this cross section of the torus is approximated in the present treatment as a rectangle, as illustrated schematically in Fig. 1(b). Here, the toroidal dust fluid is considered as confined by the effective potential $V_b(r, z)$ within the boundaries of a finite section of an infinitely long cylinder of flowing plasma, where $0 < r/L_r < 1$, $-1 < z/L_z < 1$, and $0 < \phi < 2\pi$. The effective confining potential $V_b(r, z)$ jumps from a small value within the domain to a very high value at the rectangular boundary, which serves as a rectangular equipotential line for the boundary condition of a perfect confinement.

For the azimuthally symmetric bounded dust flow that satisfies incompressible and isothermal conditions and has a

finite viscosity, the dynamics can be governed by the simplified Navier-Stokes equations in which the drive produced by the sheared ion drag and the flow resistance produced by the stationary background neutral fluid can be accounted for non-conservative vorticity sources[28]

$$\frac{\partial \mathbf{u}}{\partial t} + (\mathbf{u}\cdot\nabla)\mathbf{u} = -\frac{\nabla P}{\rho} - \nabla V_b + \mu\nabla^2\mathbf{u} - \xi(\mathbf{u}-\mathbf{v}) - \nu(\mathbf{u}-\mathbf{w}). \tag{1}$$

Here, **u**, **v,** and **w** are the flow velocities of the dust, ion, and neutral fluids, respectively. P and ρ are the pressure and mass density of the dust fluid, respectively, $V_b(r, z)$ is the confining potential, μ is the kinematic viscosity, ξ is the coefficient of ion drag acting on the dust, and ν is the coefficient of friction generated by the stationary neutral fluid.[29–31] The bounded dust clouds considered in the present analysis are within the strongly coupled as well as incompressible dust fluid regime of coupling parameter $10 \le \Gamma \le 100$. Within this regime, the elastic effects are relatively weak and negligible in comparison to the viscous effects, and thus, the simplified momentum equation is valid for the present analysis. Incompressible approximation is generally not valid in the case of weakly coupled collisionless dust fluid and gas regimes.

During the longer time scale on which the steady dust flow is maintained, all the light fluid such as electrons and ions have already been in thermal equilibrium even though it interacts or intersperses through the confined dust fluids at macroscopic fluid scales and regimes. Therefore, the steady equilibrium shear ion velocity field in Eq. (1) is valid and sufficient for the analysis of steady dust flows in the present work. Now, using the stream function-vorticity formulation discussed in the previous analysis,[23] the equations for the azimuthally symmetric steady dust flow in the two-dimensional r–z plane can be written in terms of dust stream function ($\psi\hat{\phi}$) and corresponding vorticity ($\omega\hat{\phi}$) as follows:

$$\nabla^2\psi = -\omega, \tag{2}$$

$$(\mathbf{u}\cdot\nabla)\omega = \mu\nabla^2\omega - (\xi+\nu)\omega + \xi\omega_s, \tag{3}$$

where ω_s is the external vorticity source from the unbounded sheared ion flow. Mathematically, the pressure term (∇P) appears in momentum equation with a gradient operator, denoting that the pressure acts as a conservative field, likewise the effective electrostatic confining potential (∇V_b). Further, in the stream function-vorticity formulation, the curl of conservative fields goes to zero. Therefore, the role of pressure in the present formulation has already been considered and absorbed in the velocity and vorticity equations.

In the previous work;[3] these set of Eqs. (2) and (3) have been solved analytically but only in the linear regime (Re $<$ 1), where the nonlinear inertial transport is ignored compared to the dominant diffusive transport process. It could demonstrate the analytical picture of the driven-dissipative dust vortex in terms of natural eigenmode spectrum of the system and associated scaling laws in the linear regime. Further, in the extended work,[23] the whole equations including the nonlinear inertial transport have been solved using a standard numerical approach and interpreted many of the new dust vortex characteristics in the extreme nonlinear regimes. In the previous analysis, we gave more emphasis to the nonlinear vortex characteristics at a particular bounded domain without giving the explicit detail of the numerical solution method.

Now, the details of the numerical algorithm using the method of Successive Over Relaxation (SOR)[32] and new nonlinear dust vortex characteristics in the larger flow domain relevant to some of the recent laboratory experiments are discussed in the present work. In the first step, Eqs. (2) and (3) are normalized using proper scaling units L_r and U_0, etc., such that the $\psi \to \psi/[U_0L_r]$, $\omega \to \omega/[U_0/L_r]$, $\mathbf{u} \to \mathbf{u}/[U_0]$, $\omega_s \to \omega_s/[U_0/L_r]$, $\mu \to \mu/[U_0L_r]$, $\xi \to \xi/[U_0/L_r]$, and $\nu \to \nu/[U_0/L_r]$, etc. Then, the relative importance of various terms in the equation can be compared in terms of the magnitude of the dimensionless coefficients. Now, in normalized dimensionless form, the 2-D steady incompressible Navier-Stokes equations for the dust fluid can be written as

$$0 = \nabla^2\psi + \omega, \tag{4}$$

$$0 = \nabla^2\omega - \frac{1}{\mu}(\mathbf{u}\cdot\nabla)\omega - \frac{(\xi+\nu)}{\mu}\omega + \frac{\xi}{\mu}\omega_s. \tag{5}$$

Then, the equations are cast in the form suitable for numerical solutions. Using cylindrical coordinates (r, ϕ, z) and assuming axisymmetry, Eqs. (4) and (5) can be solved in iterative steps using two residues $R_1\left(=\frac{\Delta\psi}{\Delta L^2}\right)$ and $R_2\left(=\frac{\Delta\omega}{\Delta L^2}\right)$

$$\frac{\psi^{n+1}-\psi^n}{\Delta L^2} = \left(\frac{\partial^2}{\partial r^2} + \frac{1}{r}\frac{\partial}{\partial r} - \frac{1}{r^2} + \frac{\partial^2}{\partial z^2}\right)\psi^n + \omega^n, \tag{6}$$

$$\frac{\omega^{n+1}-\omega^n}{\Delta L^2} = \left(\frac{\partial^2}{\partial r^2} + \frac{1}{r}\frac{\partial}{\partial r} - \frac{1}{r^2} + \frac{\partial^2}{\partial z^2}\right)\omega^n - \frac{1}{\mu}\left(u_r\frac{\partial\omega}{\partial r}\right)^n - \frac{1}{\mu}\left(u_z\frac{\partial\omega}{\partial z}\right)^n - K_1\omega^n + K_2\omega_s, \tag{7}$$

where $\Delta\psi \equiv \psi^{n+1} - \psi^n$ is the iterative variation, ΔL is the iteration step size (or virtual time step size), $K_1 = (\xi+\nu)/\mu$, $K_2 = \xi/\mu$, and n represents the iteration step. Since $\psi^{n+1} \to \psi^n$ for the steady state, the above equations can be rearranged as follows:

$$\left[1 - \Delta L^2\left(\frac{\partial^2}{\partial r^2} + \frac{1}{r}\frac{\partial}{\partial r} + \frac{\partial^2}{\partial z^2}\right)\right]\psi^{n+1} = \psi^n + \Delta L^2\omega^n - \frac{\Delta L^2}{r^2}\psi^n, \tag{8}$$

$$\left[1 - \Delta L^2\left(\frac{\partial^2}{\partial r^2} + \frac{1}{r}\frac{\partial}{\partial r} + \frac{\partial^2}{\partial z^2}\right)\right]\omega^{n+1} = \omega^n - \frac{\Delta L^2}{\mu}\left(u_r\frac{\partial\omega}{\partial r}\right)^n - \frac{\Delta L^2}{\mu}\left(u_z\frac{\partial\omega}{\partial z}\right)^n - \frac{\Delta L^2}{r^2}\omega^n - \Delta L^2K_1\omega^n + \Delta L^2K_2\omega_s. \tag{9}$$

For numerical efficiency, the above equations are rewritten in a two-operator form where each operator has only one directional derivative as follows:

$$\left[1-\Delta L^2\left(\frac{\partial^2}{\partial r^2}+\frac{1}{r}\frac{\partial}{\partial r}\right)\right]\left[1-\Delta L^2\frac{\partial^2}{\partial z^2}\right]\psi^{n+1} = \psi^n+\Delta L^2\omega^n-\frac{\Delta L^2}{r^2}\psi^n+\Delta L^4\left(\frac{\partial^2}{\partial r^2}+\frac{1}{r}\frac{\partial}{\partial r}\right)\left(\frac{\partial^2}{\partial z^2}\right)\psi^n, \tag{10}$$

$$\left[1-\Delta L^2\left(\frac{\partial^2}{\partial r^2}+\frac{1}{r}\frac{\partial}{\partial r}+\frac{1}{\mu}\frac{\partial\psi^n}{\partial z}\frac{\partial}{\partial r}\right)\right]\times\left[1-\Delta L^2\left(\frac{\partial^2}{\partial z^2}-\frac{1}{\mu}\left(\frac{\partial\psi^n}{\partial r}+\frac{\psi^n}{r}\right)\frac{\partial}{\partial z}\right)\right]\omega^{n+1} = \omega^n-\left(\frac{\Delta L^2}{r^2}\right)\omega^n-\Delta L^2K_1\omega^n+\Delta L^2K_2\omega_s^n+\Delta L^4\left(\frac{\partial^2}{\partial r^2}+\frac{1}{r}\frac{\partial}{\partial r}+\frac{1}{\mu}\frac{\partial\psi^n}{\partial z}\frac{\partial}{\partial r}\right)\times\left(\frac{\partial^2}{\partial z^2}-\frac{1}{\mu}\left(\frac{\partial\psi^n}{\partial r}+\frac{\psi^n}{r}\right)\frac{\partial}{\partial z}\right)\omega^n. \tag{11}$$

In order to compute the solutions on a two-dimensional grid, an initial guess on ψ_{ij}^1 and ω_{ij}^1 is made for stream function and vorticity, respectively, by additionally imposing the desired boundary conditions. In each iteration with index n, beginning from $n=1$, Eq. (10) is first solved for the radial operator part (i.e., r-part) on A_{ij}^{n+1}, which formally represents the result of the second factor in the LHS of Eq. (10) operating on the updated stream function ψ^{n+1}

$$\left[1-\Delta L^2\frac{\partial^2}{\partial z^2}\right]\psi_{ij}^{n+1}=A_{ij}^{n+1}. \tag{12}$$

The values of the computed radial operator part A_{ij}^{n+1} allow the determination of ψ_{ij}^{n+1} by inverting the axial operator part (i.e., z-part) in Eq. (12). The advantage of this process is that Eqs. (10) and (12) are reduced to tridiagonal systems which is numerically more efficient.[32]

Then, an identical procedure is applied for determining ω_{ij}^{n+1} by defining

$$\left[1-\Delta L^2\left(\frac{\partial^2}{\partial z^2}-\frac{1}{\mu}\left(\frac{\partial\psi^n}{\partial r}+\frac{\psi^n}{r}\right)\frac{\partial}{\partial z}\right)\right]\omega_{ij}^{n+1}=B_{ij}^{n+1}. \tag{13}$$

Thus, Eq. (11) is first solved for B_{ij}^{n+1}, which allows Eq. (13) to be solved for ω_{ij}^{n+1}. The updated ψ_{ij}^{n+1} values are used in the second half of the iteration to compute B_{ij}^{n+1} and ω_{ij}^{n+1}, rather than the old values ψ_{ij}^n, which concludes the nth iteration. The iterations are made by updating the ω and ψ fields until the minimum values of the residues R_1 and R_2 below a reasonably small tolerance are achieved. The relative change in errors defined by $Error = max\left(\left|\frac{\omega^{n+1}-\omega^n}{\omega^n}\right|\right)$ decreases in each iterative step down to the tolerance limit (10^{-6}), which ensures the convergence to a steady state solution as shown in Fig. 2. The iteration step ΔL, grid size Δr, and kinematic viscosity μ are the main parameters that affect the speed of convergence and numerical stability.

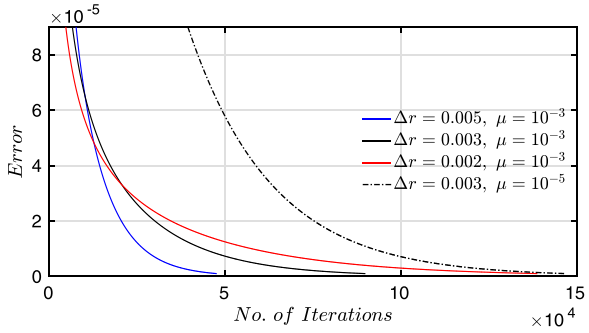

FIG. 2. Relative error as a function of iterative steps near the tolerance limit of 10^{-6} for various grid sizes $\Delta r[L_r]$ and kinematic viscosities $\mu[U_0L_r]$.

III. CHARACTERIZATION OF THE STEADY EQUILIBRIUM DUST FLOW STRUCTURE

The above equations are solved subject to proper boundary conditions. The boundary for the dust flow in the present treatment is defined by the effective potential that allows no dust flow across the confined domain where the potential V_b for dust jumps from a small accessible value to a large value at boundaries. This confinement property ($u_\perp = 0$) at the boundary gives the boundary conditions for stream function, say $\psi_{wall} = 0$. The boundary condition for ω_{wall} depends on the nature of $u_\parallel$ of the confined dust flows. A perfect slip, partial slip, and no slip are some of the common boundary conditions for $u_\parallel$. The difficulty with a vorticity-stream function formulation is the lack of natural boundary conditions in term of vorticity ω_{wall}, which, however, can be derived approximately using Thom's formula.[33]

For easy comparison with the analytic solutions presented in Refs. 3 and 4, we have used the identical conditions as the typical laboratory glow discharge argon plasma with micron-sized dust. The plasma parameters are $n \simeq 10^9\,\mathrm{cm}^{-3}$, $T_e \simeq 3\,\mathrm{eV}$, and $T_i \simeq 1\,\mathrm{eV}$ largely at the sheath entrance where ions are streaming with a flow velocity U_0 at the order of the ion acoustic velocity $c_s = \sqrt{T_e/m_i}$. Further, using the radial width of the confined domain L_r and steaming ions velocity U_0 as the ideal normalization units for the lengths and velocity of the dust flow system, the value of ion drag coefficient can be estimated as $\xi \sim 10^{-5}\,[U_0/L_r]$ and the neutral collision frequency as $\nu \sim 10^{-1}\,[U_0/L_r]$.[29–31] For a typical system size, $L_r \sim 10\,\mathrm{cm}$, the range of kinematic viscosity μ can similarly be chosen as $\mu \sim 10^{-6}\,[U_0L_r]$ which corresponds to the small Reynolds numbers (Re ≈ 1) of the dust flow in the linear viscous regime.[3]

A. Benchmark of the numerical solutions

The present model for dust clouds is generic and applicable to many of driven-dissipative dynamic equilibrium systems. It has the freedom of choice for the external driver, i.e., the background ion flow, and the nature of boundary of the confining domain. However, for direct comparison with the previous analytic solutions,[3] now we consider the same physical conditions, especially the same external driving field. The flow profile of streaming ions is specified as

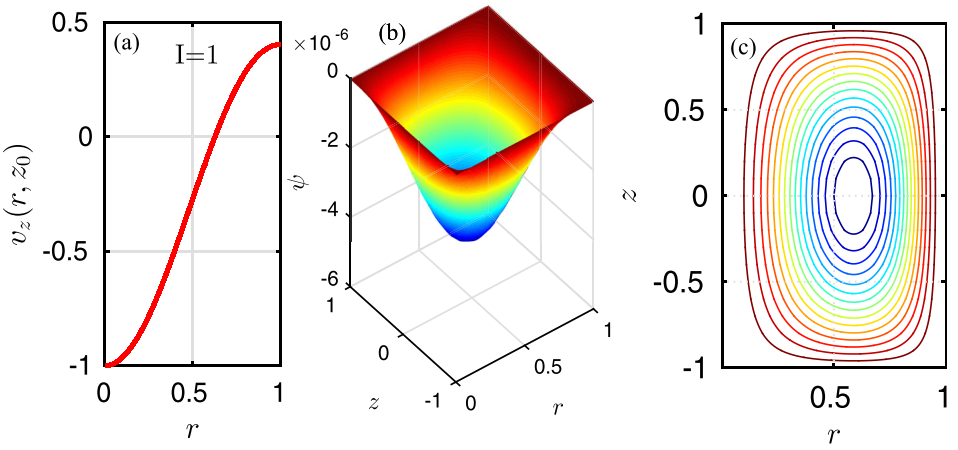

FIG. 3. (a) Driver ion velocity flow profile $v_z(r, z)$ with axial and radial shears in the $z = z_0$ cross section, (b) 2D stream function $\psi(r, z)$ of the dust flow, and (c) corresponding streamlines for the dust fluid flow in the $r - z$ cross section for system parameters $\mu = 1 \times 10^{-3}[U_0 L_r]$, $\xi = 1 \times 10^{-5}[U_0/L_r]$ and $\nu = 1 \times 10^{-1}[U_0/L_r]$.

$$v_z(r, z) = A_m J_0\left(\alpha_I \frac{r}{L_r}\right)\cos\left(\frac{\pi z}{2L_z}\right). \tag{14}$$

Here, A_m is the magnitude of the external driving field. The radial modes are determined by the I_{th} root of Bessel function $J_1(\alpha_I) = 0$ at the external boundary. The axial mode $k_z = (\pi/2L_z)$ specifies a single vortex along the axial direction as in experimental observations.[21] The numerical solution for the stream function $\psi(r, z)$ and its corresponding streamlines (i.e., the contours of the product $r\psi$) in the linear viscous regime are shown in Figs. 3(b) and 3(c), respectively, for $\mu = 10^{-3}[U_0 L_r]$, $\xi = 10^{-5}[U_0/L_r]$, and $\nu = 10^{-1}[U_0/L_r]$. This streamline pattern shows similar characteristic features of low-Re dust flow as in Ref. 3, where the flow is the anti-clockwise circulation, axially symmetric, and aligned to the confining boundary, ensuring vorticity transport purely due to diffusion orthogonal to the streamlines.

A more quantitative comparison is possible between the flow velocity component profiles obtained numerically and those from analytic solutions in the linear limit.[3] The profiles of the dust flow velocity components, i.e., $u_z(r, z_0)$ and $u_r(r_0, z)$, passing through the center of the circulation (r_0, z_0) are compared for the kinematic viscosity varying from $\mu = 10^{-1}$ *to* $\mu = 10^{-5}[U_0 L_r]$ in the linear regime (Re $\ll 1$) (Fig. 4). In the highly viscous regimes, the dust fluid flows with a velocity in the range of 0.1–1 mm/s in the confined domain. The analytical and numerical results are in good agreement. The above comparisons show the validity of the numerical method and motivate for further analysis of the driven dust flow characteristics at higher Reynolds number nonlinear regimes. Further, the variations in velocity profiles for $u_r(r_0, z)$ and $u_z(r, z_0)$ near the boundary indicates the impact of boundary conditions and the formation of a boundary layer in particular. Boundary layers are formed due to the effective viscous stress on flow due to boundaries. The thickness of the boundary layer decreases with kinematic viscosity as shown in Figs. 4(a)–4(c). Thus, at a higher Reynolds number, the thickness of the boundary layer is negligibly small as $\Delta r_b \simeq \mu^{1/3}$,[3] and reduces to a very thin layer giving sharp deviation in velocity profile as shown in Fig. 4(f). There is no boundary layer formation for the perfect slip boundary conditions as shown in Figs. 4(d)–4(f).

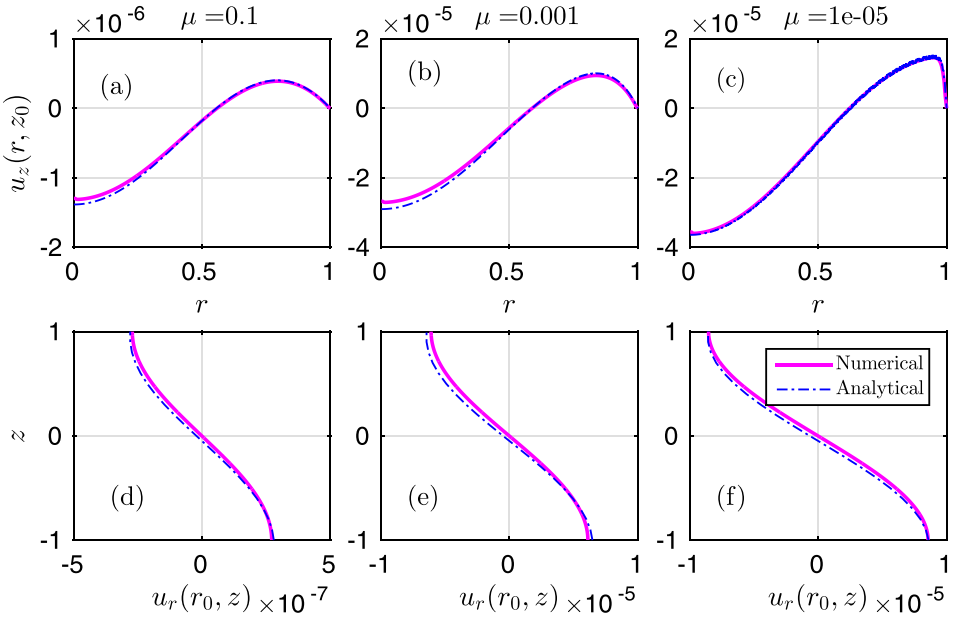

FIG. 4. Comparison between analytical and numerical solutions of $u_r(r_0, z)$ *and* $u_z(r, z_0)$ for fixed system parameters, $\xi = 1 \times 10^{-5}[U_0/L_r]$, $\nu = 1 \times 10^{-1}[U_0/L_r]$, and varying $\mu = 10^{-1}$ *to* $10^{-5}[U_0 L_r]$ in the linear regimes Re $\ll 1$.

B. Emerging nonlinear characteristics in the steady equilibrium dust flow structures

When the contribution of nonlinear advection transport $(\mathbf{u}\cdot\nabla)\mathbf{u}$ is included in the higher Reynolds number regimes, the momentum of dust flow increases enormously, and it becomes important to maintain a low driver ion velocity so that Mach number of the dust $M_d = u/c_{sd} \ll 1$ for incompressible flow in practice. Thus, for the study of nonlinear effects at higher Re regimes, the driver ions stream with a shear flow velocity U_0 equivalent to a fraction of the ion acoustic speed c_s. The order of kinematic viscosity corresponding to small Reynolds numbers (Re $\simeq$ 1) of dust flow becomes $\mu \sim 10^{-4}\,[U_0 L_r]$ which is consistent with the linear viscous regime. The corresponding ion drag coefficient can be estimated as $\xi \sim 10^{-4}\,[U_0/L_r]$ and neutral collision frequency as $\nu \sim 10^{-3}\,[U_0/L_r]$ for further analysis.[29–31]

Now, the above flow analysis of the bounded driven dust flow dynamics is extended to high Re regimes. The streamlines of 2D steady dust flow in the linear and nonlinear regimes are presented in Fig. 5 for the radial mode numbers $I = 1$ and 3 of the same driver flow. The flow structures are analyzed for two important cases of kinematic viscosity, i.e., $\mu = 10^{-3}[U_0 L_r]$ for the linear regime and $\mu = 10^{-5}[U_0 L_r]$ for the nonlinear regime which corresponds to flow regimes Re $\approx$ 0.001 and Re $\approx$ 50.0, respectively. In these regimes, the dust fluid flows within the velocity range of 1–50 mm/s, while the dust acoustic speed c_{sd} is found to be 12 cm/s in the domain. As observed in the earlier analysis,[3,4] the flow structure in the linear regime is characterized by a system of symmetric and elongated circulations (or streamlines that are aligned with the confining boundaries) as shown in Fig. 5 (2nd column). The alternating positive and negative shear in the external driving field in case of $I = 3$ leads to the formation of counter-rotation in addition to scales introduced by the confining boundary and stationary background fluid.[3] However, in the nonlinear regime, as shown in Fig. 5 (3rd column), the flow structure changes into an asymmetric and elongated circulation with a finite displacement of the center of circulation $(\mathbf{u}(\mathbf{r_0}, \mathbf{z_0}) = \mathbf{0})$. In the case of multiple vortices (in the $I = 3$ case), the circulation center shifts along with the driver. In many dusty plasma experiments,[16,21] similar multiple dust vortices are observed to correlate with the scales of the ion dragging interaction in the background. Further, a remarkable property of the present analysis is that the geometry and the dimension of steady driven dust vortex structure in the linear regime are mainly asserted by the confining boundary, whereas, in the nonlinear regime, the structure is mostly controlled by the dynamical regime rather than the boundary. Interestingly, a similar kind of vortex dynamics and asymmetric structural transition with the varying system parameters is observed in some of the recent dusty plasma experiments.[19,20] The asymmetric structure in the nonlinear regime is the main reason for the emergence of the localized highly shear layers and isolated regions of acceleration and frictional retardation of the flow fields in the higher velocity regime of the dusty plasma experiments.[21,22]

C. Flow structure dependence on the dynamical regime and domain aspect ratio

The influence of various system parameters or dynamical regimes on vortex structure is further analyzed explicitly for the $I = 1$ case (Fig. 5, 1st row). For the driven-dissipative system, the steady state momentum equation can be written as

$$(\mathbf{u}\cdot\nabla)\mathbf{u} = -\frac{\nabla P}{\rho} - \nabla V + \mu\nabla^2\mathbf{u} - \xi(\mathbf{u}-\mathbf{v_s}) - \nu(\mathbf{u}-\mathbf{w_n}).$$

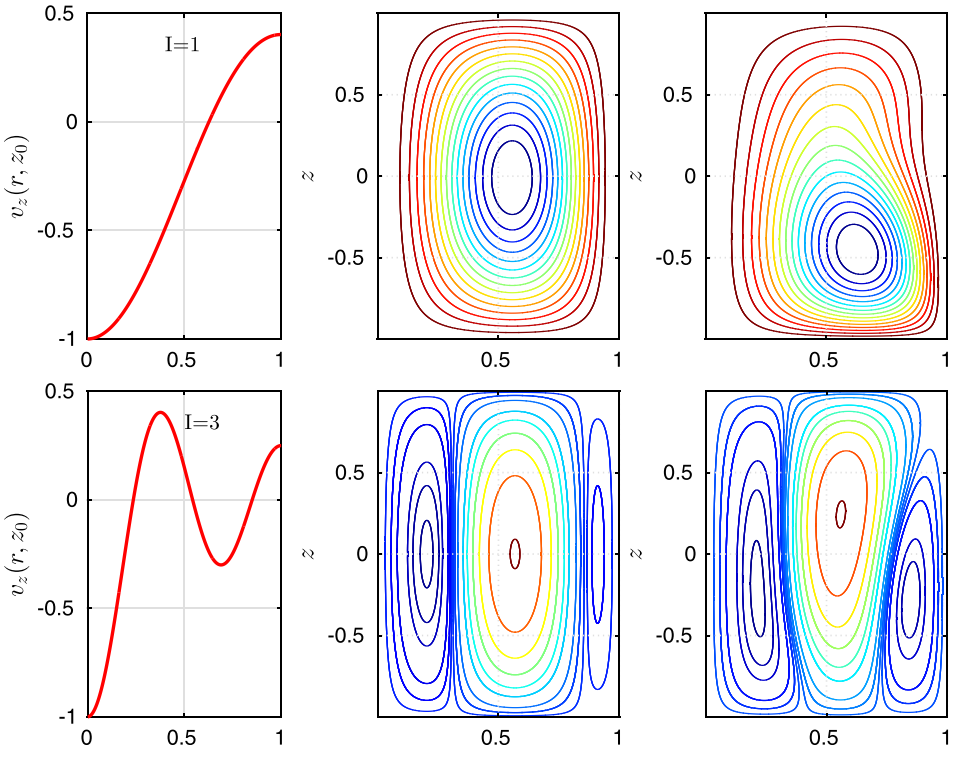

FIG. 5. (1st column) Driver ion's velocity profile at $z = z_0$ for radial sheared mode numbers $I = 1$ *and* 3. The corresponding streamlines pattern for the dust fluid flows in the $r - z$ cross section for (2nd column) $\mu = 10^{-3}[U_0 L_r]$ and (3rd column) $\mu = 3 \times 10^{-5}[U_0 L_r]$ is shown.

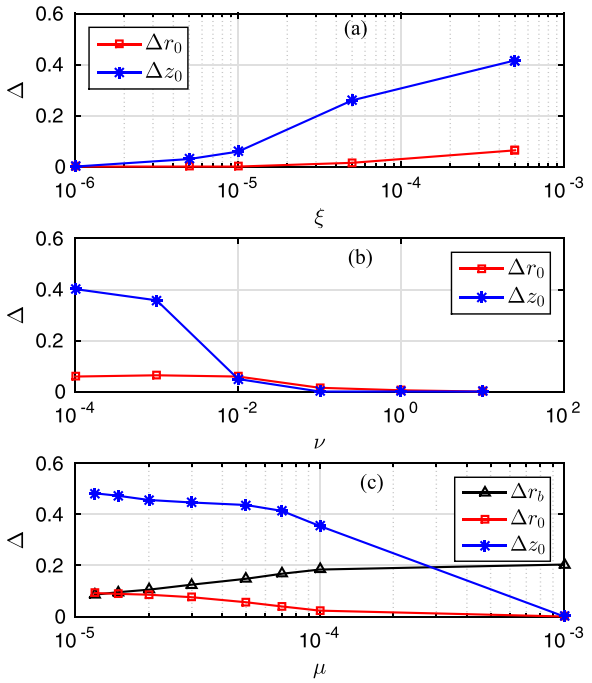

FIG. 6. Shift of the circulation center (r_0, z_0) as a function of (a) ion dragging co-efficient ξ, (b) neutral collision frequency ν, and (c) kinematic viscosity μ. The boundary layer thickness Δr_b as a function of μ is also plotted in (c).

Applying the condition for the center of circulation, i.e., $\mathbf{u}(\mathbf{r_0}, \mathbf{z_0}) = \mathbf{0}$, the equation at ($r_0$, z_0) reduces to

$$\frac{\nabla P}{\rho} + \nabla V - \mu \nabla^2 \mathbf{u} = \xi \mathbf{v_s} + \nu \mathbf{w_n}. \tag{15}$$

Here, P is the dynamic pressure of the incompressible flow which becomes a function of velocity $\mathbf{u}$, which again depends on μ. V is the effective confining potential and the diffusion transport $\mu\nabla^2\mathbf{u}$ at the center point (r_0, z_0) is negligibly small. Now, Figs. 6(a) and 6(b) show the radial and axial shifts of the center point (r_0, z_0) with respect to ξ and ν, respectively. The radial shift Δr_0 is small in each case, while the axial shift Δz_0 with ξ, ν is high in the higher Reynolds regime. However, in the case of μ variation shown in Fig. 6(c), the shift Δz_0 increases slowly in the higher Re regime. Further, the radial shift Δr_0 and the change in boundary layer thickness Δr_b due to varying kinematic viscosity μ correlate with each other. Therefore, the variation in radial shift Δr_0 with the kinematic viscosity can also be used as an additional scale for the estimation of kinematic viscosity of charged fluids using the appropriate scaling law $\mu \sim \Delta r_b^3$ and $\mu \sim \Delta r_b^2 \left(\frac{u}{L_\parallel}\right)$, discussed in the previous work.[3,23] Moreover, the different variations in radial and axial shifts of the center of circulation (r_0, z_0) with respect to system parameters suggest that the steady flow structure also depends on the aspect ratio (L_z/L_r) of the confined domain. This may be because in the nonlinear regime, $(\mathbf{u}\cdot\nabla)\mathbf{u}$ introduces new scale $L_\parallel \sim (u/u')$ in addition to the diffusion scale ($L_\perp$). The analysis of nonlinear flow characteristics in a domain of unity aspect-ratio ($L_z/L_r = 1$)[23,34] shows that the shifting in both the Δz_0 and Δr_0 is relatively small and similar.

IV. SUMMARY AND CONCLUSIONS

The 2D hydrodynamical model from the previous work[23] is employed to demonstrate the structural transition from linear to nonlinear regimes for a driven-dissipative dust cloud confined in an azimuthally symmetric toroidal system in dynamic equilibrium with an unbounded streaming plasma. The detailed procedure for the numerical solutions of the 2D hydrodynamical model is discussed, which are benchmarked with the analytical solution in the linear regime.[3]

Our results show the role of Re number for the convective transport process in the linear to nonlinear regimes, and how the symmetry of structure varies with system parameters. The vortex structure symmetry of the steady dust fluid in the poloidal cross section of higher aspect-ratio ($L_z/L_r = 2$) is analyzed within the transition range of Reynolds number $0.001 < Re \leq 50$ where the dust flow with speed ranges from 0.1 mm to 5 cm while the corresponding dust acoustic speed is about 12 cm/s. It has been observed that the geometry and dimension of the steady dust vortex in the linear regime ($\mathrm{Re} \leq 1$) are mainly determined by confining boundaries, whereas it is governed by the dynamics (or dynamical regime) rather than the boundaries in the nonlinear regime ($\mathrm{Re} \gg 1$). Thus, the steady dust flow structure in the linear regime is characterized by symmetric and elongated vortices with various scales mainly introduced by the driving fields and boundaries. However, at $\mathrm{Re} \gg 1$, the steady dust flow structure is no longer symmetric. Instead, a new asymmetric and elongated structure appears with scales mainly dependent on the driven-dissipation parameters such as ξ, ν, and μ in addition to the aspect ratio of the confined domain. The asymmetric structure in the higher Re regime generates strong local sheared and isolated regions for the acceleration and frictional retardation of the flow, which is relevant to observations in various dusty plasma experiments. In addition to the asymmetric dust flow structures in the high Reynolds number regime, we find that the radial shift of the center of circulation of the steady dust flows exhibits the tendency of following scaling law, which can be used for estimating the kinematic viscosity of the charged fluids.

It is concluded that steady driven and bounded dust flow in an unbounded streaming plasma can possess various flow structures in linear and nonlinear dynamic regimes depending on scales introduced mainly by non-uniformity of the unbounded external driving field and the system parameters including the nature of the confining boundaries. The numerical model is generic and applicable to other driven-dissipative systems such as the microscopic biological system and the gigantic Jovian vortices. Further analysis of the nonlinear flow characteristics and its stability in various aspect-ratios of flow domain and arbitrary Re regimes will be reported in future publications.

ACKNOWLEDGMENTS

The author L. Modhuchandra thanks Dr. Devendra Sharma and late Professor P. K. Kaw, Institute for Plasma Research, India, for the invaluable support and encouragement all the time. This research was supported by the State Administration

of Foreign Experts Affairs—Foreign Talented Youth Introduction Plan under Grant No. WQ2017ZGKX065 and the National Magnetic Confinement Fusion Program of China under Grant Nos. 2014GB124002 and 2015GB101004. The author P. Zhu also acknowledges the support from U.S. Department of Energy under Grant Nos. DE-FG02-86ER53218 and DE-FC02-08ER54975. This work used resources of the Supercomputing Center of University of Science and Technology of China.

[1]L. Holzer, J. Bammert, R. Rzehak, and W. Zimmermann, Phys. Rev. E **81**, 041124 (2010).
[2]S. Grossmann, Rev. Mod. Phys. **72**, 603 (2000).
[3]M. Laishram, D. Sharma, and P. K. Kaw, Phys. Rev. E **91**, 063110 (2015).
[4]M. Laishram, D. Sharma, and P. K. Kaw, Phys. Plasmas **21**, 073703 (2014).
[5]E. Lauga and T. R. Powers, Rep. Prog. Phys. **72**, 096601 (2009), available at http://stacks.iop.org/0034-4885/72/i=9/a=096601.
[6]C. W. Wolgemuth, Biophys. J. **95**, 1564 (2008).
[7]L. Pan, A. Morozov, C. Wagner, and P. E. Arratia, Phys. Rev. Lett. **110**, 174502 (2013).
[8]Y. Paul, T. Edwards, E. Fu, K. Helton, K. Nelson, M. R. Tam, and B. H. Weigl, Nature (London) **442**, 412 (2006).
[9]T. M. Squires and S. R. Quake, Rev. Mod. Phys. **77**, 977 (2005).
[10]A. D. Stroock, S. K. W. Dertinger, A. Ajdari, I. Mezić, H. A. Stone, and G. M. Whitesides, Science **295**, 647 (2002).
[11]J. Sommaria, S. D. Meyers, and H. L. Swinney, Nature (London) **331**, 689 (1988).
[12]D. S. Choi, D. Banfield, P. Gierasch, and A. P. Showman, Icarus **188**, 35 (2007).
[13]P. S. Marcus, J. Fluid Mech. **215**, 393–430 (1990).
[14]N. Nivedita, P. Ligrani, and I. Papautsky, Sci. Rep. **7**, 44072 (2017).
[15]S. Hamaguchi, R. T. Farouki, and D. H. E. Dubin, Phys. Rev. E **56**, 4671 (1997).
[16]V. N. Tsytovich, G. Morfill, U. Konopka, and H. Thomas, New J. Phys. **5**, 66 (2003).
[17]K.-B. Chai and P. M. Bellan, Phys. Plasmas **23**, 023701 (2016).
[18]M. Choudhary, S. Mukherjee, and P. Bandyopadhyay, Phys. Plasmas **24**, 033703 (2017).
[19]S. Mitic, R. Sütterlin, A. V. I. H. Höfner, M. H. Thoma, S. Zhdanov, and G. E. Morfill, Phys. Rev. Lett. **101**, 235001 (2008).
[20]T. H. Hall and E. Thomas, IEEE Trans. Plasma Sci. **44**, 463 (2016).
[21]M. Kaur, S. Bose, P. K. Chattopadhyay, D. Sharma, J. Ghosh, Y. C. Saxena, and E. Thomas, Jr., Phys. Plasmas **22**, 093702 (2015).
[22]M. Kaur, S. Bose, P. K. Chattopadhyay, D. Sharma, J. Ghosh, and Y. C. Saxena, Phys. Plasmas **22**, 033703 (2015).
[23]M. Laishram, D. Sharma, P. K. Chattopadhyay, and P. K. Kaw, Phys. Rev. E **95**, 033204 (2017).
[24]M. Klindworth, A. Melzer, A. Piel, and V. A. Schweigert, Phys. Rev. B **61**, 8404 (2000).
[25]S. Mitic, B. A. Klumov, U. Konopka, M. H. Thoma, and G. E. Morfill, Phys. Rev. Lett. **101**, 125002 (2008).
[26]M. A. Fink, S. K. Zhdanov, M. Schwabe, M. H. Thoma, H. Höfner, H. M. Thomas, and G. E. Morfill, EPL (Europhys. Lett.) **102**, 45001 (2013).
[27]O. Arp, D. Block, M. Klindworth, and A. Piel, Phys. Plasmas **12**, 122102 (2005).
[28]L. Landau and E. Lifshitz, *Fluid Mechanics* (Elsevier Science, 2013), Vol. 6.
[29]M. S. Barnes, J. H. Keller, J. C. Forster, J. A. O'Neill, and D. K. Coultas, Phys. Rev. Lett. **68**, 313 (1992).
[30]S. A. Khrapak, A. V. Ivlev, G. E. Morfill, and H. M. Thomas, Phys. Rev. E **66**, 046414 (2002).
[31]A. V. Ivlev, S. A. Khrapak, S. K. Zhdanov, G. E. Morfill, and G. Joyce, Phys. Rev. Lett. **92**, 205007 (2004).
[32]W. H. Press, *The Art of Scientific Computing* (Cambridge University Press, 1992).
[33]E. Weinan and J.-G. Liu, J. Comput. Phys. **124**, 368 (1996).
[34]M. Laishram, D. Sharma, P. K. Chattopdhyay, and P. K. Kaw, AIP Conf. Proc. **1925**, 020028 (2018).